Structure 14, 1241–1249, August 2006 ©2006 Elsevier Ltd All rights reserved DOI 10.1016/j.str.2006.06.007

The Open State Gating Mechanism of Gramicidin A Requires Relative Opposed Monomer Rotation and Simultaneous Lateral Displacement

Gennady V. Miloshevsky[1] and Peter C. Jordan[1,*]
[1] Department of Chemistry
MS-015 Brandeis University
P.O. Box 549110
Waltham, Massachusetts 02454

Summary

The gating mechanism of the open state of the gramicidin A (gA) channel is studied by using a new Monte Carlo Normal Mode Following (MC-NMF) technique, one applicable even without a target structure. The results demonstrate that the lowest-frequency normal mode (NM) at ~6.5 cm^{-1} is the crucial mode that initiates dissociation. Perturbing the gA dimer in either direction along this NM leads to opposed, nearly rigid-body rotations of the gA monomers around the central pore axis. Tracking this NM by using the eigenvector-following technique reveals the channel's gating mechanism: dissociation via relative opposed monomer rotation and simultaneous lateral displacement. System evolution along the lowest-frequency eigenvector shows that the large-amplitude motions required for gating (dissociation) are not simple relative rigid-body motions of the monomers. Gating involves coupling intermonomer hydrogen bond breaking, backbone realignment, and relative monomer tilt with complex side chain reorganization at the intermonomer junction.

Introduction

Many proteins have multiple open and closed states. Analysis of the conformational transitions between these states poses a major challenge in computationally relating structure and function (Woolf et al., 2004). A protein undergoes repeated oscillation in its extended minimum energy well before concentrating sufficient energy, far in excess of the thermal energy, in the "reaction coordinate"; thus, it can then overcome the barrier and cross from an open to a closed state (or vice versa). Such structural transitions occur only infrequently; they are highly improbable and are known as rare events (Passerone et al., 2003; Allen et al., 2006). The molecular dynamics approach (Karplus and McCammon, 2002; Gumbart et al., 2005), a traditional theoretical tool for investigating protein flexibility, is not a practical way to study rare phenomena such as cooperative and large-amplitude conformational transitions. The real time required to reliably simulate such processes is far greater than present computational resources permit. The best theoretical method for studying collective motions in proteins is normal mode analysis (NMA), which describes dynamics in terms of collective variables, the normal mode (NM) coordinates (Levitt et al., 1985). The low-frequency NMs obtained from NMA can provide a first approximation of the gating pathway between the closed and open states of a protein.

Gramicidin A (gA) is a simple hydrophobic peptide that dimerizes to form cation channels in lipid bilayers (Urry et al., 1971). Its gating is thought to involve monomer association and dissociation (Woolley and Wallace, 1992; Durkin et al., 1993; Goulian et al., 1998; Lundbæk and Andersen, 1999). The hydrophobic length of the dimeric gA channel generally differs from the unperturbed membrane's thickness. A channel opens (conducts) when monomers associate head-to-head at their N termini, spanning the membrane, which deforms in response. The dimer is stabilized by six strong, intermonomer hydrogen bonds (HBs). The deformed membrane stresses the dimer junction axially, promoting channel dissociation. It is believed that at the transition state two HBs are broken, i.e., the monomers have moved 1.6 Å apart (Lundbæk and Andersen, 1999). However, the kinetic behavior of gA is considerably more complex than suggested by this simple two-state model. Dimer formation and dissociation is sensitive to membrane lipid composition and channel-bilayer hydrophobic mismatch. "Mini-channels" with multiple, relatively low conducting states have been proposed (Busath and Szabo, 1981), but later work indicated that these effects reflected environmental contamination (the source of lipid, gramicidin, and electrolyte solution) affecting channel structure (Busath et al., 1987; Sawyer et al., 1989). However, bilayer thickness unquestionably influences the conformational preference of gA channels; in thick bilayers, the equilibrium between single-stranded (SS) and double-stranded (DS) dimers shifts to favor the DS state (Mobashery et al., 1997). In addition, with increased channel-bilayer mismatch SS gA channels exhibit a new lower-conductance state arising from repeated association and dissociation of the same pair of monomers (Mobashery et al., 1997). Furthermore, very brief closing events in single-channel recordings suggest the presence of short-lived, nonconducting states; these appear to be structurally closely related to the conducting dimer (Ring, 1986; Sigworth et al., 1987). Recently, multiple intermediate conformational states of gA single channels were directly observed (Harms et al., 2003) via a new approach, patch-clamp fluorescence microscopy (PCFM), which measures single-molecule fluorescence spectra and records single-channel currents simultaneously (Harms et al., 2004). It was postulated that the multiple intermediate conformers mainly reflect fluctuations of the six intermonomer HBs, disrupting the dimeric pore's structure. Single-molecule PCFM imaging measurements provided unambiguous evidence that the gA channel could be in closed (nonconducting) states for hundreds of milliseconds, even if the two monomers are still in an intermediate dimerized state, without significant change in their physical separation (Lu, 2005).

Gross structural details of dimer dissociation were revealed in a computational study (Miloshevsky and Jordan, 2004a, 2004b) with the kinetic Monte Carlo

*Correspondence: jordan@brandeis.edu

Reaction Path Following method (Miloshevsky and Jordan, 2005). This method samples large-scale conformational transitions along a predefined degree of freedom. Thus, it requires as input a well-defined reaction coordinate. We postulated that the relative rotation angle of gA monomers is a proper reaction coordinate, i.e., one for which recrossings do not occur, and we studied the relative translational and rotational motion of the rigid monomers, with one of them space fixed. This simplified model captured essential features of dissociation dynamics and showed that a mobile monomer undergoes relative rotation with simultaneous lateral displacement rather than direct axial separation (Miloshevsky and Jordan, 2004a). Axial separation was energetically far more costly than this rotary-lateral motion. Our analysis also predicted that, in thick membranes, hydrophobic mismatch greatly aids the formation of open-pore states with four and two intermonomer HBs. In transiting between these states, the conductance is interrupted as the monomers undergo a relative rotational and lateral shift.

Here, our focus is the gating mechanism of the gA open state. To obtain atomistic understanding, we developed a new, to our knowledge, theoretical approach, Monte Carlo Normal Mode Following (MC-NMF) (Miloshevsky and Jordan, 2006). It does not require having both initial and target conformations, being applicable if only one stable state is known. This method combines NMA (Levitt et al., 1985) and the eigenvector-following (EF) technique (Baker, 1986; Nichols et al., 1990) with the Metropolis Monte Carlo method (Metropolis et al., 1953). An NM-based Monte Carlo protocol for folding small helical proteins was also recently reported (Wu et al., 2005). In this protocol, a random walk is based on elastic NMs, with energies computed by using a new knowledge-based potential function rather than the Hooke's law potential typical of elastic NMA. The central feature of NMA is its ability to predict directions for potential conformational changes. The course of structural change along the low-frequency NMs is unique, and it is predominantly determined by the shape of the protein (Lu and Ma, 2005). Large-scale intrinsic motions that run counter to NMs are structurally forbidden. Many studies have clearly shown that proteins follow pathways coupling one or a few low-frequency NMs in transiting between functionally important states (for a review, see Ma [2005] and references therein). Therefore, we associate the direction established by the lowest-frequency NM with the gating transition, eliminating the need for a predetermined reaction coordinate (Miloshevsky and Jordan, 2004a). However, NMs do not describe the absolute displacement amplitude for any group of atoms. Low-frequency NMs are only a first approximation to the gating pathway connecting closed and open states. Typically, a target structure is generated from an initial structure by atomic displacements along the eigenvector of the lowest-frequency NM until a preset root-mean-square deviation (rmsd), typically 2–3.5 Å, between the two structures is attained (Shen et al., 2002; Taly et al., 2005; Cheng et al., 2006). This opening-closing motion is only valid in interpreting the initial stages of gating and of facilitating factors (e.g., ligand binding) that give rise to the actual gating transition. Without a target crystal structure, there is no guarantee that energy barriers are entirely crossed and that conformational endpoints are properly connected.

The major limitation of NMA is that it studies dynamics in a particular conformation, one that describes a local minimum on a potential energy surface (PES). NMA descriptions of protein dynamics near stationary points can only complement other methods in studying gating transitions. Therefore, we use EF (Nichols et al., 1990) to establish gating pathway(s) and transition-state structures of gA. To the best of our knowledge, the application of EF to systems as large and flexible as ion channel proteins is entirely novel. Previous studies were limited to finding transition states in molecules and small atomic clusters. We generate transition-state structures of gA by constructing a properly ordered sequence of steps moving energetically uphill along the lowest-frequency NM while simultaneously minimizing the energy along all other NMs (Baker, 1986; Nichols et al., 1990). Minima are found by stepping downhill in all normal coordinates. The Metropolis criterion (Metropolis et al., 1953) determines allowable moves. Sampling is Boltzmann weighted. Thermal fluctuations spread the set of transition pathways, so different MC-NMF runs yield an ensemble of transition-state structures. These transition-state searches are computationally expensive; after each accepted move, the Hessian matrix is recalculated and rediagonalized. However, the great advantage of this approach is that it gives detailed information about gA's behavior, especially its dynamics, gating pathway rearrangements, and structural transformations. Our results demonstrate that the lowest-frequency NM at $\sim$6.5 cm^{-1} is the crucial mode that initiates dissociation. Tracking this NM by using the EF technique reveals the channel's gating mechanism: dissociation via relative opposed monomer rotation and simultaneous lateral displacement.

Results

Two high-resolution, lipid-solvated gA structures, 1JNO and 1MAG (Townsley et al., 2001; Ketchem et al., 1996), were used, and standard all-mode NMA was carried out in vacuum on each for empty channels and for ones doubly ion occupied, with seven water molecules and a K^+ ion in each binding site. This latter assembly (the 1JNO structure, two K^+ ions, and seven waters), shown in Figure 1, is termed the "1JNO system." A "1MAG system" was constructed similarly.

Hessian of gA

There are $N = 575$ atoms in each gA system, resulting in 1725 NMs. It is interesting to visualize the systems' Hessians. Figure 2 depicts the Hessian elements on a square grid for the minimized 1JNO system (Figure 1), calculated in a Cartesian representation. The largest elements are concentrated along and near the diagonal. All off-diagonal Hessian elements are negligible with respect to those near the diagonal. Recently, Lu and Ma (2005) showed that the low-frequency subspace of eigenvectors (which dominate concerted structural change) is robustly similar, even upon complete randomization of the (non-zero) Hessian matrix elements, as long as the structure of the matrix (the positions of the non-zero and zero elements) is maintained. Intrigued by this

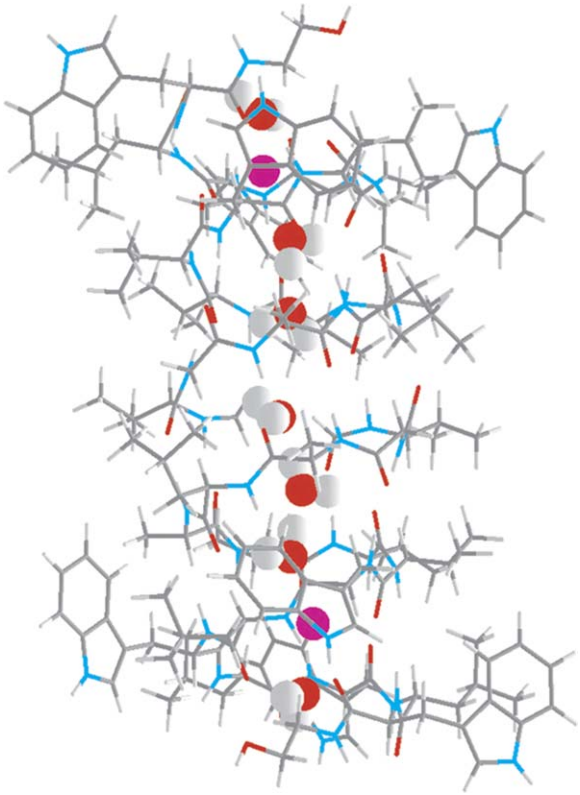

Figure 1. The Minimized 1JNO Structure Is Shown as Sticks

Two K^+ ions at their binding sites are shown as pink spheres. Seven waters, five in the pore between the ions and two exterior in the pore mouths, are included. The assembly, based on the 1JNO structure, two K^+ ions, and seven waters, is termed the "1JNO system." The "1MAG system" is constructed similarly. The figure was generated by using our MCICP code.

fact, we tested the errors introduced by the exclusion of small elements in the Hessian matrix by setting elements below a predetermined threshold equal to zero. If we keep only the Hessian elements bigger than 0.001 kcal/(mol·Å^2), i.e., store only 65.3% of the Hessian, eigenvalues and eigenvectors are essentially unaltered. We also obtain reasonable results by setting the threshold at 0.01 kcal/(mol·Å^2), i.e., storing only 27.1% of the Hessian. However, the eigenvalue and eigenvector calculations failed when the threshold was set at 0.1 kcal/(mol·Å^2), meaning that important matrix elements had been discarded. Results were even better if matrix elements smaller than the chosen threshold were generated randomly from a uniform distribution rather than being set to zero. These results imply that a huge number of Hessian elements need not be stored, an observation of great practical importance in application to large proteins.

NMs of gA

The two gA original structures, with 73 and 45 negative eigenvalue modes in 1JNO and 1MAG, respectively, reorganize noticeably when energy minimized in vacuum. The basic aim of this minimization was to determine a gA geometry with the lowest strain energy. EF determines a minimal strain energy geometry by proceeding downhill along all NMs until an rms gradient of $\sim 10^{-6}$ kcal mol^{-1} Å^{-1} is reached. To establish the geometry with the least strain energy, all degrees of freedom (bond lengths, bond angles, torsion, and improper torsion angles) in both gA and the waters were variable. The first six eigenvalues of the minimized gA structures are zero; all others are positive, as required at a minimum. The corresponding eigenvectors are 3*N*-dimensional vectors (NMs) specifying the directions of the change in the minimum-energy gA conformation; the eigenvalues quantify the energetic cost of deformation along these directions. For both 1JNO and 1MAG systems, the lowest-frequency NM is $\sim$6.5 cm^{-1}. This corresponds to 0.0186 kcal/mol (1 kcal/mol = 349.75 cm^{-1}), or 0.0312 kT at 300K. The energy drop in minimization is $\sim$328.1 kT for the 1JNO structure and $\sim$669.4 kT for

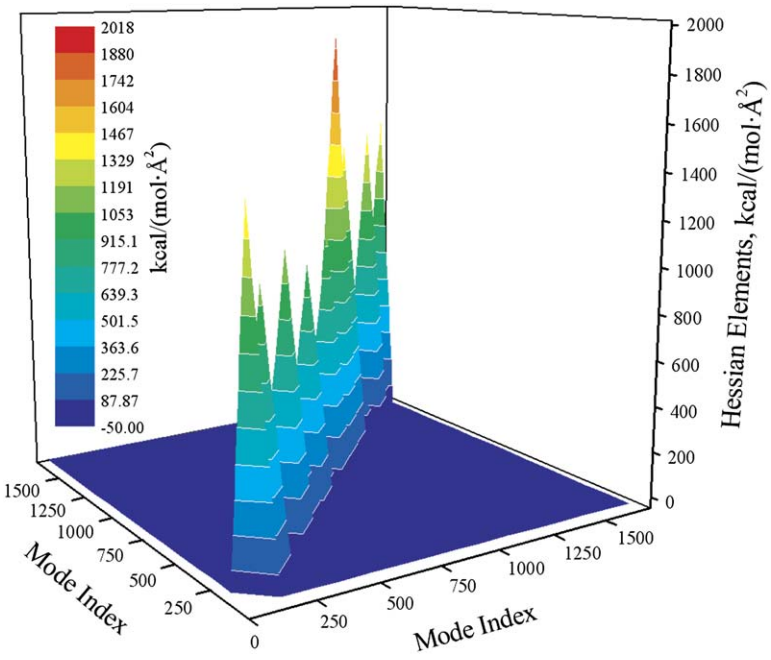

Figure 2. The Elements of a Hessian Matrix for the Minimized 1JNO System on a 1725 × 1725 Grid

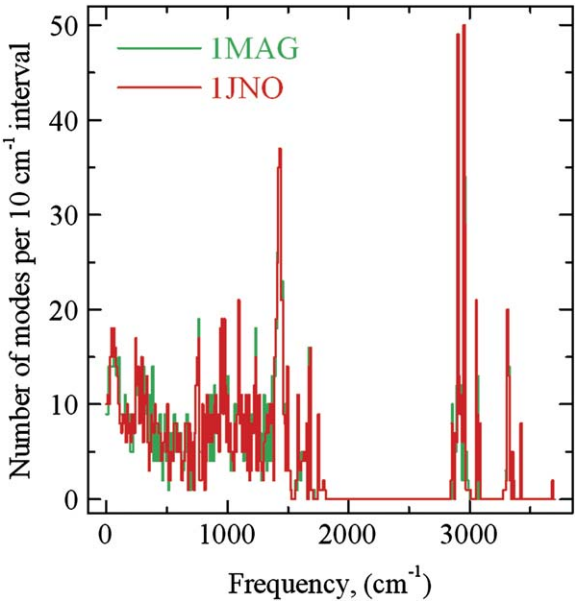

Figure 3. The Frequency Spectrum of the 1JNO and 1MAG Systems

the 1MAG structure, indicating that 1JNO is less stressed than 1MAG. Low-frequency eigenvalues of both gA structures and gA systems differ little, demonstrating that the pore contents only marginally influence the energetic cost of deformation along low-frequency eigendirections. Low-frequency eigenvectors were basically unaltered by the presence of the ions and waters in the gA pore and should also be representative of behavior in a channel occupied by a single ion.

The calculated NM frequency spectra are shown in Figure 3. As most NMs describe motions common to all proteins, different proteins exhibit very similar frequency spectra. Motions specific to a particular protein, and thus central to understanding its function, are at a spectrum's low end. At low frequencies the spectrum mimics that of Roux and Karplus (Roux and Karplus, 1988), with ~18 modes in the interval 50–60 cm^{-1}; these describe motions of secondary, β sheet-like, structure elements. At higher frequencies (>500 cm^{-1}) our NM spectrum differs from theirs (Roux and Karplus, 1988), which was based upon an idealized model of gA differing importantly from both 1JNO and 1MAG structures. The region from 500 to 1800 cm^{-1} corresponds to internal vibrations of single amino acids. Differences between 1JNO and 1MAG spectra reflect slight side chain conformational variability between the two structures. The well-separated block of hydrogen-heavy atom vibrations, absent in (Roux and Karplus, 1988), appears at large wave numbers (>2800 cm^{-1}).

Rmsd between the gA Structures

The 1JNO and 1MAG structures, MC-NMF-minimized in vacuum, converge in a way similar to those simulated in a lipid bilayer (Allen et al., 2003). The initial rmsd between 1JNO and 1MAG backbones/whole structures of 1.4/3.1 Å decreases to 0.35/2.3 Å for the minimized structures (backbone rmsds from the first and last nanosecond of MD simulations were 0.36 Å and 0.21 Å, respectively [Allen et al., 2003]). We find that the rmsds between the minimized 1MAG structure and the crystal 1MAG structure (1.35/2.48 Å) are much higher than those for 1JNO (0.58/0.91 Å). The MD simulations (Allen et al., 2003) also found much greater change in the 1MAG backbone (1.2 Å) than in 1JNO (0.63 Å). The 1MAG structure is highly stressed compared to the 1JNO structure (the energy drops more, and the rmsd is larger), in agreement with the conclusions of Allen et al. (2003). However, the transition of Trp9 between the 1JNO and 1MAG orientations (Allen et al., 2003) was not observed in our MC-NMF minimization. This may reflect the fact that the Trp9 transitions are environment dependent.

Low-Frequency NMs of the 1JNO and 1MAG Systems from All-Mode NMA

We computed all NMs of gA and selected the seventh one, the lowest non-zero eigenvalue. It was studied in its two opposite directions. Perturbation of the 1JNO system (Figure 4A) along the lowest-frequency eigenvector (seventh) in "negative" (Figure 4B) or "positive" (Figure 4C) directions reveals the relative rotation of the gA monomers, behavior also observed for the 1MAG system. This is nearly pure rigid-body rotation around the pore axis, with the monomers rotating in opposite directions. In a "negative" rotational displacement (Figure 4B), the blue monomer rotates clockwise, and the green one rotates anticlockwise. "Positive" rotations (Figure 4C) reverse directionality. Near both channel mouths, the monomers distend slightly, and atomic displacements are larger than at the intermonomer junction. In moving along the seventh eigenvector, the 1MAG monomers are less rigid than the 1JNO

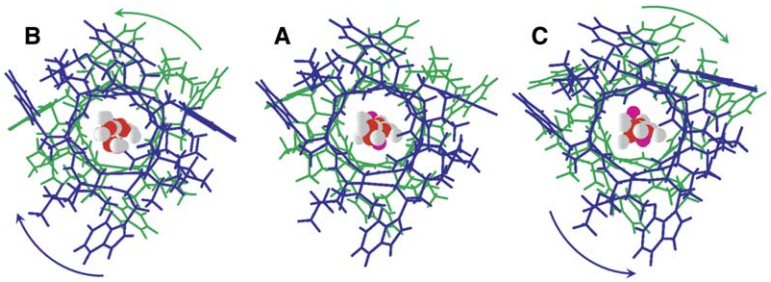

Figure 4. Displacement of the Atoms of the 1JNO System along the Eigenvector of the Lowest-Frequency Collective Mode, the Seventh Overall, in the Two Opposing Directions Termed "Negative" and "Positive"

(A) The minimized 1JNO system, as viewed along the channel axis. gA monomers are colored blue and green. Ions and waters are shown in the pore.

(B) The gA system displaced along the seventh eigenvector in the "negative" direction. Blue and green arrows show the direction of motion of each monomer.

(C) The gA system displaced along the seventh eigenvector in the "positive" direction.

The figures were generated with our MCICP code.

monomers. For both the 1JNO and the 1MAG systems, perturbation along the eighth eigenvector led to relative monomer tilt, with neither case well described as rigid body monomer motion. Large rigid-body monomer blocks, especially those near the channel mouths that include a number of Trp residues, exhibit larger-amplitude vibration than those near the intermonomer junction. Perturbation along higher-frequency NMs leads to complex relative rigid-body motions of large atomic groups.

The next two sections describe low-frequency NMs calculated by using coarse-grained approaches (RTB and Elastic Network Model), and, to assess the utility of these approximate models, compares them with low-frequency NMs computed via all-mode NMA. These methods calculating a limited number of low-frequency NMs cannot be used to compute gating pathways (the transition-state conformations section), as we find that high-frequency NMs, especially those of the torsional subspace, are crucial in mapping the gating pathways.

Low-Frequency NMs of the 1JNO and 1MAG Structures from the RTB Approach

In the RTB (rotations-translations of blocks) method (Tama et al., 2000), low-frequency NMs are described as pure rigid-body motions of blocks of consecutive amino acid residues. Dividing the 1JNO and 1MAG structures into rigid blocks, of one residue each, yields a total of $n_b = 34$ blocks and 204 RTB NMs. Approximate low-frequency NMs were found by diagonalizing the RTB matrix, which is much smaller, $6n_b \times 6n_b$, than the all-atom Hessian matrix, $3N \times 3N$. The RTB eigenvalues overestimate the energetic cost of deformation along low-frequency NMs, but at low frequencies they correlate well with the all-mode eigenvalues, scaled by ~1.7. The overlaps between the approximate RTB and the all-mode eigenvectors for the three lowest-frequency NMs of 1JNO are 0.97, 0.43, and 0.54, respectively. For the three lowest-frequency NMs of 1MAG, the corresponding overlaps are 0.99, 0.98, and 0.83. The two sets of lowest-frequency NMs from the approaches are very similar, especially the seventh eigenvector. Displacement of the minimized 1JNO and 1MAG structures along the seventh RTB eigenvector in both the "negative" and "positive" directions revealed totally concerted, relative opposed monomer rotations. Thus, the RTB method very accurately approximates the lowest-frequency NM; the all-mode NMA seventh eigenvector is reliably described as a pure rigid-body motion of blocks of consecutive gA residues. The one residue per block RTB approach is 13 times faster than the standard all-mode NMA; memory requirements are correspondingly greatly reduced.

The Lowest-Frequency NM of the 1JNO Structure from the Elastic Network Model

ElNémo (Suhre and Sanejouand, 2004), a web interface to the Elastic Network Model, was used to calculate the lowest-frequency NM of the 1JNO structure and to generate perturbed 1JNO structures along the seventh eigenvector. The structural model of 1JNO perturbed along the seventh eigenvector in both the "negative" and "positive" directions showed relative axial opposed monomer rotations. Although *ElNémo* uses a single-parameter Hookean potential, the seventh eigendirection seems as accurate as that obtained with the all-atom CHARMM22 force field. However, the eigenvalues are even larger than those obtained from the RTB approach.

Transition-State Conformations

We tracked the lowest-frequency all-mode NMA eigenvector in the "positive" direction by using EF. Following the seventh eigenvector yields multiple minima and transition-state conformers with one negative eigenvalue indicative of a saddle point. Stationary points (minima and saddle points) on transition pathways are geometries with the lowest strain energy in all modes, i.e., their gradients are zero. Figures 5A and 5B show a particular example of the transition-state conformer (saddle point) obtained from the minimized 1JNO system (Figure 2) by tracking the lowest-frequency eigenvector. The negative eigenvalue corresponds to an imaginary frequency, $8.1i$ cm^{-1}. The energy difference between minimized and saddle point 1JNO systems is ~19.7 kT. Monomers rotate in opposite directions with simultaneous lateral displacement that occludes the pore. Complex transitions that rearrange side chains and reconfigure the gA backbone are observed. Initially, the ^{1}H-^{5}O and ^{5}O-^{1}H bonds rupture. As monomers continue to rotate, the ^{1}O-^{5}H bond also breaks, resulting in the transition-state structure (Figures 5A and 5B). The monomers are linked by the three remaining HBs (^{3}H-^{3}O, ^{3}O-^{3}H, and ^{5}H-^{1}O). At the intermonomer junction, the pore is distorted and monomers are displaced laterally (Figure 5B). The next minimum on the transition pathway is only ~2 kT, more stable than the transition-state conformer of Figures 5A and 5B. At this local minimum on the transition path, the structure of the 1JNO system (not shown) differs slightly from that at the saddle point. The next saddle point (transition-state conformer not shown) is ~25.7 kT less stable than the previous local minimum conformer. The negative eigenvalue corresponds to the imaginary frequency, $5.0i$ cm^{-1}. Here, the ^{5}H-^{1}O bond has broken, and only the ^{3}H-^{3}O and ^{3}O-^{3}H bonds link the monomers. The relative lateral displacement is larger than in Figure 5B. The last minimum found on the transition pathway was ~14 kT lower in energy. No further saddle points were found, and the monomers dissociate laterally, as seen in Figures 5C and 5D, agreeing with our earlier predictions (Miloshevsky and Jordan, 2004a).

MC-NMF simulations of the 1JNO and 1MAG systems exhibit multiple dissociation pathways. Metropolis Monte Carlo simulates natural thermal fluctuational processes, which significantly ease the crossing of small energy barriers. The gating transition proceeds with complex side chain reorganization and relative monomeric tilt. As side chains sample a rich rotameric space, multiple gating pathways are possible. These pathways are similar to conformational transitions seen in adenylate kinase (Miyashita et al., 2003) that exhibit transition paths and an ensemble of transition-state structures. The 1MAG system dissociated directly without forming transition-state conformers. We also saw HB breaking within a 1MAG monomer, with corresponding monomer unraveling; the dimer linkage remained intact. Flash movies illustrating dynamic dissociation details are

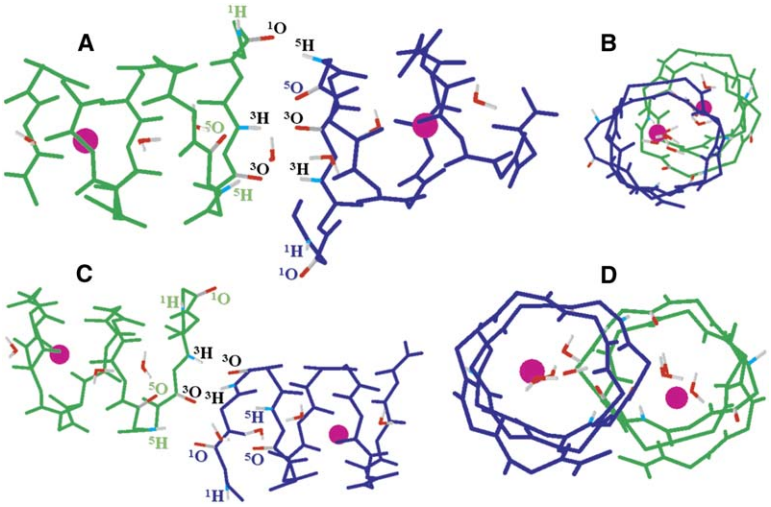

Figure 5. Structural Geometry of the 1JNO System at its First Saddle Point and the Dissociation State Conformation of the 1JNO System

(A–D) Views are within a plane and along the channel axis. For clarity, only the backbone, ions, and waters are shown. H and O atoms in black type refer to junction atoms with intact HBs. Figures were generated with our MCICP code.

(A) View of saddle point geometry within a plane.

(B) View of saddle point geometry along the channel axis.

(C) View of dissociation state conformation within a plane.

(D) View of dissociation state conformation along the channel axis. Monomers are fully displaced laterally.

found at http://people.brandeis.edu/~gennady/gA_NormalModes.html. Thus, detailed transition pathways differ, not only between the 1JNO and 1MAG systems, but also among 1JNO and 1MAG systems originating from different MC-NMF runs. The gating pathway shown in Figure 5 was reproduced repeatedly. However, the definitive observation is that in each of our MC-NMF simulations, dissociation gating of the gA channel arises by relative opposed monomer rotation followed by lateral displacement.

Discussion

It is known that low-frequency NMs, while strongly damped by solvent, describe functionally relevant conformational transitions in proteins (Ma, 2005). We have developed a method for studying gating and other slow conformational transitions of biomolecules that is practical, even if structural data are only available for the initial state. Application to gA showed that the crucial collective mode for gating is the lowest-frequency NM at $\sim$6.5 cm^{-1}. Perturbing the gA dimer in either direction along this NM leads to opposed, nearly rigid-body rotations of the gA monomers around the central pore axis. This was demonstrated in three ways: all-mode NMA, the RTB method, and the Elastic Network Model. Channel gating is due to coupled relative monomer rotation and lateral displacement. Initially, the atomic perturbation along the seventh eigenvector leads to relative axial opposed monomer rotations. Lateral displacement arises later, during EF, along the lowest-frequency NM. This gating mechanism, discovered by using a new MC-NMF approach in which the direction defined by the lowest-frequency NM is associated with the transition pathway, agrees perfectly with our earlier predictions (Miloshevsky and Jordan, 2004a) based on the simplified computational model (Miloshevsky and Jordan, 2005) in which the rotation angle, ϕ, between gA monomers provides a good initial guess for the gating pathway. The MC-NMF approach predicts relative opposed rotation of gA monomers, a particular feature not visible from our earlier computational study (Miloshevsky and Jordan, 2004a) in which one monomer was space fixed. Relative monomer rotations with short-range lateral displacements lead to natural fluctuations in the pore cross-section at the dimer junction, consistent with very brief interruptions in the current signal (Ring, 1986). Later measurements (Heinemann and Sigworth, 1990) revealed current fluctuations with dwell times of $\sim$3 μs, in excess of "shot noise," which were interpreted as being due to internal motions of the channel protein. Our results (see Figure 5) also demonstrate that the channel can be trapped in metastable states, in which monomers only partially dissociated. This finding is consistent with the existence of hidden closed states with periods of hundreds of milliseconds (Harms et al., 2003)—states that are not observable in conventional single-channel patch recordings. Several well-separated, brief closing events on the time scale of tens of milliseconds are also seen in the single-channel trace of the Cs^+ current through the gA channel (Heinemann and Sigworth, 1990).

The generally accepted gating model (Lundbæk and Andersen, 1999) suggests that two conformational states are involved in gA's open-closed transition. The channel is totally open when the dimer is fully associated; the channel is closed when the two monomers are separated. However, recent experimental results (Harms et al., 2003; Lu, 2005) show that, in addition to its conventional open and closed states, gA can also exist in multiple intermediate conformational states. The channel could be closed even if the intermonomer distance did not change significantly, i.e., if the monomers were still dimerized. However, the structures of the intermediate conformational states and the atomic details of the structure-activity relationship were not revealed experimentally. Our theoretical results complement these data (Harms et al., 2003) suggesting the mechanism of gating and providing structural and molecular insight into how the channels function. The two essential features of the gating mechanism, opposed monomer rotation and simultaneous lateral displacement, are inherent to every gating pathway (e.g., direct dissociation and monomer breakage) identified in the MC-NMF simulations. Following the lowest-frequency eigendirection showed that real large-amplitude motions associated

with gating are not simple relative rigid-body monomer motions. Before backbone realignment can occur, it is imperative to reorganize the side chains at the intermonomer junction and alter relative monomer tilt. Contrasting protein NMA in dihedral space and Cartesian space (Kitao et al., 1994) showed that bond length and angle fluctuations mainly lead to greater dihedral angle flexibility. These fluctuations are responsible for the ~13% difference between the rmsds in low-frequency modes determined from dihedral and Cartesian space (Kitao et al., 1994). This highlights the importance of using all-mode NMA, including relaxation of bond angles and lengths, to properly describe protein gating transitions.

If only a few low-frequency NMs are implicated in the large-scale conformational transitions, the RTB method can be reliably used to identify potential conformational changes for a particular application. As frequency increases, the overlap between approximate RTB and standard all-mode NM eigenvectors rapidly deviates from unity and is very small at larger frequencies. Therefore, the RTB NMs cannot be used to map the gating pathway, as relaxing high-frequency NMs, especially those of the torsional subspace, is absolutely essential.

Our NMA studies and EF along the lowest-frequency NM of the gA systems are, like almost all other NMA studies, performed in vacuum. How will lipid and water surroundings alter the direction of observed gating transitions? It is known that large-amplitude motions in a realistic environment are strongly overdamped and diffusive in nature, not vibrational at all, which makes low frequencies of little physical significance (Kitao et al., 1991; Ma, 2005). However, there is compelling evidence that the native directionality of structural changes in proteins is not affected by the presence of solvent or the use of highly simplified potential functions (Ma, 2005). Intrinsic motions that counter NMs are structurally forbidden. The directions of structural change along NMs are unique for each protein, and protein shape predominates in determining the eigenvectors of low-frequency NMs (Lu and Ma, 2005). Thus, only eigendirections are meaningful, not the timescales and amplitudes of low-frequency motions derived from the related eigenvalues, which are simply used to sort NMs in order of increasing energy. Therefore, we conclude that the predicted gating mechanism in gA systems will not change when surrounded by lipid and water, as this is an inherent property of gA architecture. Here, we found that low-frequency eigenvectors are unaffected by the ions and waters in the pore. Our previous study (Miloshevsky and Jordan, 2004a) showed that the channel-bilayer hydrophobic mismatch has no discernable effect on dimer behavior in the 6HB state, even for thick membranes, as changes in the intermonomer interaction energy (large increase) and the elastic energy of the membrane deformation (small decrease) are highly incompatible. However, the specifics of the gating pathways, especially their later stages, are sensitive to their surroundings. When two intermonomer HBs break, hydrophobic mismatch greatly affects the dissociation pathway(s), leading to the formation of 4HB and even 2HB conducting states in a thick membrane (Miloshevsky and Jordan, 2004a). In the absence of a mismatch, we found (Miloshevsky and Jordan, 2004a) that the dimer dissociates laterally (without forming a 4HB state), consistent with our current results. Gating occurs when the gA system and its surroundings concentrate a significant amount of the thermal energy in the lowest-frequency eigendirection, the transition pathway with the minimal energy cost, to mount the barrier and cross from the open to the closed state.

Experimental Procedures

The gA systems were described with the standard CHARMM22 topology and parameter files (MacKerell et al., 1998), and all calculations were carried out in vacuum. The CHARMM potential energy, E_c, was approximated as a harmonic function, E_h, of the atomic mass-weighted Cartesian coordinates, $\mathbf{x}$, around a stable conformation, $\mathbf{x}_0$, by using a Taylor expansion:

$$E_h(\mathbf{x}) \approx E_c(\mathbf{x}_0) + \mathbf{g}^T(\mathbf{x}-\mathbf{x}_0) + \tfrac{1}{2}(\mathbf{x}-\mathbf{x}_0)^T\mathbf{H}(\mathbf{x}-\mathbf{x}_0), \quad (1)$$

where $\mathbf{g}$ is the mass-weighted gradient vector, and $\mathbf{H}$ is the mass-weighted Hessian matrix. For the bond and nonbonding energy terms, the first and second derivatives of the potential energy, E_c, with respect to the mass-weighted Cartesian coordinates were calculated analytically. For other energy terms (angle, dihedral, improper, and Urey-Bradley terms), a modification of the Ridders' method of polynomial extrapolation (Ridders, 1982), a fourth-order, finite-difference differentiation, was used to calculate the first and second derivatives numerically. The error in double precision, which is $\sim 10^{-14}$, was comparable to the machine accuracy (10^{-16}).

NMs (a total of 1725) of the gA systems were obtained through the standard diagonalization of the Hessian matrix, the $3N \times 3N$ matrix of the second derivatives of the potential energy, E_c, with respect to the mass-weighted Cartesian coordinates, where $N = 575$ is the number of atoms in the gA system. The eigensolver DSPEV from the LAPACK library (Anderson et al., 1999) was used to calculate the Hessian's eigenvalues and the corresponding eigenvectors. To achieve high-performance, highly optimized "building block" BLAS routines (Dongarra et al., 1990) for performing basic vector and matrix operations were used.

The essential features of our MC-NMF method are as follows. NMA expresses the protein dynamics in terms of collective variables, the NM coordinates (Levitt et al., 1985). Normal coordinates describe structure-inherent collective displacements of protein atoms. We use normal coordinates as a well-suited coordinate reference frame for studying properties of a PES of the gA system. The EF technique (Nichols et al., 1990) was applied to establish gating pathways and to find saddle points. All simulations were performed at 300 K. As NMA is performed at nonstationary points on the transition pathway, the overall translational and rotational modes that arise from a Hessian matrix, $\mathbf{H}$, were removed by using the Eckart conditions (Eckart, 1935), which fix the center of mass in space and constrain infinitesimal rotations of the dimer. Mode-following was initiated by a short Newton-Raphson step, $\mathbf{h}_{NR} = -\sum_{i=1}^{3N} \bar{g}_i \mathbf{V}_i/\lambda_i$, where $\bar{g}_i$ is the component of the gradient $\mathbf{g}$ along the eigenvector $\mathbf{V}_i$, and λ_i is the i^{th} eigenvalue; $\mathbf{h}_{NR}$ is small and variable, typically ranging from ~0.1 to ~1.0 Å. A positive eigenvalue, $\lambda_i > 0$, leads to a decrease in the harmonic energy, $\Delta E_h = -\frac{1}{2}\sum_{i=1}^{3N} \bar{g}_i^2/\lambda_i$, along the associated $\mathbf{V}_i$ eigendirection, and a negative eigenvalue, $\lambda_i < 0$, leads to the energy increase. The transition states (saddle points) on a PES were found by systematically maximizing the energy along the lowest-frequency eigenvector of the Hessian while simultaneously minimizing the energy along all other orthogonal eigendirections (Nichols et al., 1990). Initially, the lowest-frequency eigenvalue is positive. Sign inversion indicates that motion along this eigenvector now describes uphill displacement toward a maximum. All other eigenvalues remain positive, and motions along these eigendirections are downhill to a minimum. The local (or global) minima can be located within the same framework by minimizing the energy along all NMs. New mass-weighted coordinates, $\mathbf{x}$, are sampled as $\mathbf{x} = \mathbf{x}_0 + \xi \cdot \mathbf{h}_{NR}$; ξ is randomly chosen between 0 and 1. The moves along the gating pathway associated with the step $\xi \cdot \mathbf{h}_{NR}$ were accepted with a probability of $\min[1, \exp(-\Delta E_c/kT)]$ (Metropolis et al., 1953), where ΔE_c is the change in the energy calculated by using the CHARMM22 potential energy function. Note that the full

CHARMM energy change, ΔE_c, is used, not the harmonic approximation, ΔE_h. This Metropolis step is similar to that used in a Monte Carlo analysis performed by Wu et al. (2005), in which the full energy change is also evaluated, by using a Hamiltonian superior to the simple Hooke's law potential typical of elastic network studies. However, in our approach, we follow the lowest-frequency eigenvector(s) calculated from the all-mode NMA by using the EF technique. If a new configuration, **x**, is accepted, then we replace $\mathbf{x}_0$ by **x**; rebuild the Hessian matrix; recalculate gradients, eigenvectors, and eigenvalues; and continue the EF process. Eigenvalues change as we move along the transition pathway, resulting in a smooth change of eigendirections. The eigenvalue of the mode being followed drops. We choose the eigenvector corresponding to the smallest eigenvalue to follow further. As overall translational and rotational motions of the gA system are removed by using the Eckart conditions (Eckart, 1935), this procedure allows for proper switching between eigendirections to ensure that the desired lowest eigenvalue uphill eigenvector corresponding to the lowest energetic cost is properly identified. Conformational change is not always driven by the same NM. At some points on the transition pathway, the lowest-frequency NM describes a relative tilt of gA monomers, not their opposed rotation. This MC-NMF technique, before its application to the gA systems, was extensively tested to find minima and saddles in acetic acid and hexane molecules.

The RTB matrix H_b (size $6n_b \times 6n_b$) was constructed from the all-atom Hessian **H** (size $3N \times 3N$), $H_b = P^T H P$, with P the $3N \times 6n_b$ projection matrix built of vectors associated with local rotation and translation of each block (Tama et al., 2000). The approximate eigenvalues, E_b, and eigenvectors, U_b, of the gA structures in the RTB subspace are obtained by diagonalizing H_b by using the standard DSPEV eigensolver (Anderson et al., 1999). The ($3N$) eigenvectors, U, in the atomic space were obtained from the approximate RTB eigenvectors, U_b, by using the projection matrix as $U = PU_b$.

All of these techniques were implemented in our MCICP (Monte Carlo Ion Channel Proteins) code. All MC-NMF simulations are performed by using the MCICP code.

This MC-NMF methodology can be used to study ion-channel protein conformational dynamics and gating mechanisms in more complex systems. To economize in applying the MC-NMF method to large proteins with no loss of detail, we plan to introduce smart eigensolvers like ARPACK (Lehoucq et al., 1998), which relies heavily on LAPACK (Anderson et al., 1999) and BLAS (Dongarra et al., 1990), both implemented in our MCICP code. ARPACK reduces the number of floating point operations and eigenvector matrix storage needs. It is designed to focus on a small, particularly significant set of eigenvalues and their corresponding eigenvectors, such as the first M low-frequency NMs. Storage requirements are then $O(N \times M)$, not $O(N^2)$. More importantly, the entire Hessian matrix need not be stored in memory, and its factorization is obviated. Only a Hessian-vector product (Lehoucq et al., 1998), which requires $O(N)$ floating point operations, not $O(N^2)$, is needed.

Acknowledgments

We thank Benoît Roux for providing us with NMs of the water molecule for testing our NMA technique at its implementation stage. This work was supported by grant GM-28643 from the National Institutes of Health.

Received: April 6, 2006
Revised: June 1, 2006
Accepted: June 9, 2006
Published: August 15, 2006

References

Allen, R.J., Frenkel, D., and ten Wolde, P.R. (2006). Simulating rare events in equilibrium or non-equilibrium stochastic systems. J. Chem. Phys. *124*, 024102.

Allen, T.W., Andersen, O.S., and Roux, B. (2003). Structure of gramicidin A in a lipid bilayer environment determined using molecular dynamics simulations and solid-state NMR data. J. Am. Chem. Soc. *125*, 9868–9877.

Anderson, E., Bai, Z., Bischof, C., Blackford, S., Demmel, J., Dongarra, J., Du Croz, J., Greenbaum, A., Hammarling, S., McKenney, A., and Sorensen, D. (1999). LAPACK Users' Guide, Third Edition (Philadelphia, PA: SIAM).

Baker, J. (1986). An algorithm for the location of transition states. J. Comput. Chem. *4*, 385–395.

Busath, D., and Szabo, G. (1981). Gramicidin forms multi-state rectifying channels. Nature *294*, 371–373.

Busath, D.D., Andersen, O.S., and Koeppe, R.E., II. (1987). On the conductance heterogeneity in membrane channels formed by gramicidin A. A cooperative study. Biophys. J. *51*, 79–88.

Cheng, X., Lu, B., Grant, B., Law, R.J., and McCammon, J.A. (2006). Channel opening motion of $\alpha 7$ nicotinic acetylcholine receptor as suggested by normal mode analysis. J. Mol. Biol. *355*, 310–324.

Dongarra, J.J., Du Croz, J., Hammarling, S., and Duff, I.S. (1990). A set of level 3 basic linear algebra subprograms. ACM Trans. Math. Soft. *16*, 1–17.

Durkin, J.T., Providence, L.L., Koeppe, R.E., II, and Andersen, O.S. (1993). Energetics of heterodimer formation among gramicidin analogues with an NH_2-terminal addition or deletion: consequences of a missing residue at the join in channel. J. Mol. Biol. *231*, 1102–1121.

Eckart, C. (1935). Some studies concerning rotating axes and polyatomic molecules. Phys. Rev. *47*, 552–558.

Goulian, M., Mesquita, O.N., Fygenson, D.K., Nielsen, C., Andersen, O.S., and Libshaber, A. (1998). Gramicidin channel kinetics under tension. Biophys. J. *74*, 328–337.

Gumbart, J., Wang, Y., Aksimentiev, A., Tajkhorshid, E., and Schulten, K. (2005). Molecular dynamics simulations of proteins in lipid bilayers. Curr. Opin. Struct. Biol. *15*, 423–431.

Harms, G.S., Orr, G., Montal, M., Thrall, B.D., Colson, S.D., and Lu, H.P. (2003). Probing conformational changes of gramicidin ion channels by single-molecule patch-clamp fluorescence microscopy. Biophys. J. *85*, 1826–1838.

Harms, G.S., Orr, G., and Lu, H.P. (2004). Probing ion channel conformational dynamics using simultaneous single-molecule ultrafast spectroscopy and patch-clamp electric recording. Appl. Phys. Lett. *84*, 1792–1794.

Heinemann, S.H., and Sigworth, F.J. (1990). Open channel noise. V. Fluctuating barriers to ion entry in gramicidin A channels. Biophys. J. *57*, 499–514.

Karplus, M., and McCammon, J.A. (2002). Molecular dynamics simulations of biomolecules. Nat. Struct. Biol. *9*, 646–652.

Ketchem, R.R., Lee, K.C., Huo, S., and Cross, T.A. (1996). Macromolecular structural elucidation with solid-state NMR-derived orientational constraints. J. Biomol. NMR *8*, 1–14.

Kitao, A., Hirata, F., and Go, N. (1991). The effects of solvent on the conformation and the collective motions of protein: normal mode analysis and molecular dynamics simulations of melittin in water and in vacuum. Chem. Phys. *158*, 447–472.

Kitao, A., Hayward, S., and Go, N. (1994). Comparison of normal mode analyses on a small globular protein in dihedral angle space and Cartesian coordinate space. Biophys. Chem. *52*, 107–114.

Lehoucq, R.B., Sorensen, D.C., and Yang, C. (1998). ARPACK Users' Guide: Solution of Large-Scale Eigenvalue Problems with Implicitly Restarted Arnoldi Methods (Philadelphia: SIAM).

Levitt, M., Sander, C., and Stern, P.S. (1985). Protein normal-mode dynamics: trypsin inhibitor, crambin, ribonuclease and lysozyme. J. Mol. Biol. *181*, 423–447.

Lu, H.P. (2005). Probing single-molecule protein conformational dynamics. Acc. Chem. Res. *38*, 557–565.

Lu, M., and Ma, J. (2005). The role of shape in determining molecular motions. Biophys. J. *89*, 2395–2401.

Lundbæk, J.A., and Andersen, O.S. (1999). Spring constants for channel-induced lipid bilayer deformations. Estimates using gramicidin channels. Biophys. J. *76*, 889–895.

Ma, J. (2005). Usefulness and limitations of normal mode analysis in modeling dynamics of biomolecular complexes. Structure *13*, 373–380.

MacKerell, A.D., Jr., Bashford, D., Bellott, M., Dunbrack, R.L., Jr., Evanseck, J.D., Field, M.J., Fischer, S., Gao, J., Guo, H., Ha, S., et al. (1998). All-atom empirical potential for molecular modeling and dynamics studies of proteins. J. Phys. Chem. B *102*, 3586–3616.

Metropolis, N., Rosenbluth, A., Rosenbluth, M., Teller, A., and Teller, E. (1953). Equation of state calculations by fast computing machines. J. Chem. Phys. *21*, 1087–1091.

Miloshevsky, G.V., and Jordan, P.C. (2004a). Gating gramicidin channels in lipid bilayers: reaction coordinates and the mechanism of dissociation. Biophys. J. *86*, 92–104.

Miloshevsky, G.V., and Jordan, P.C. (2004b). Permeation in ion channels: the interplay of structure and theory. Trends Neurosci. *27*, 308–314.

Miloshevsky, G.V., and Jordan, P.C. (2005). Permeation and gating in proteins: kinetic Monte Carlo reaction path following. J. Chem. Phys. *122*, 214901–214907.

Miloshevsky, G.V., and Jordan, P.C. (2006). Gating transitions in proteins: Monte Carlo normal mode following. Biophys. J. *90*, Suppl. 2791-Pos.

Miyashita, O., Onuchic, J.N., and Wolynes, P.G. (2003). Nonlinear elasticity, proteinquakes, and the energy landscapes of functional transitions in proteins. Proc. Natl. Acad. Sci. USA *100*, 12570–12575.

Mobashery, N., Nielsen, C., and Andersen, O.S. (1997). The conformational preference of gramicidin channels is a function of lipid bilayer thickness. FEBS Lett. *412*, 15–20.

Nichols, J., Taylor, H., Schmidt, P., and Simons, J. (1990). Walking on potential energy surfaces. J. Chem. Phys. *92*, 340–346.

Passerone, D., Ceccarelli, M., and Parrinello, M. (2003). A concerted variational strategy for investigating rare events. J. Chem. Phys. *118*, 2025–2032.

Ridders, C.J.F. (1982). Accurate computation of F′(x) and $F'(x)$ $F''(x)$. Adv. Eng. Softw. *4*, 75–76.

Ring, A. (1986). Brief closures of gramicidin A channels in lipid bilayer membranes. Biochim. Biophys. Acta *856*, 646–653.

Roux, B., and Karplus, M. (1988). The normal modes of the gramicidin-A dimer channel. Biophys. J. *53*, 297–309.

Sawyer, D.B., Koeppe, R.E., and Andersen, O.S. (1989). Induction of conductance heterogeneity in gramicidin channels. Biochemistry *28*, 6571–6583.

Shen, Y., Kong, Y., and Ma, J. (2002). Intrinsic flexibility and gating mechanism of the potassium channel KcsA. Proc. Natl. Acad. Sci. USA *99*, 1949–1953.

Sigworth, F.J., Urry, D.W., and Prasad, K.U. (1987). Open channel noise. III. High-resolution recordings show rapid current fluctuations in gramicidin A and four chemical analogues. Biophys. J. *52*, 1055–1064.

Suhre, K., and Sanejouand, Y.-H. (2004). *ElNémo*: a normal mode web server for protein movement analysis and the generation of templates for molecular replacement. Nucleic Acids Res. *32*, W610–W614.

Taly, A., Delarue, M., Grutter, T., Nilges, M., Novère, N.L., Corringer, P.-J., and Changeux, J.-P. (2005). Normal mode analysis suggests a quaternary twist model for the nicotinic receptor gating mechanism. Biophys. J. *88*, 3954–3965.

Tama, F., Gadea, F.X., Marques, O., and Sanejouand, Y.-H. (2000). Building-block approach for determining low-frequency normal modes of macromolecules. Proteins *41*, 1–7.

Townsley, L.E., Tucker, W.A., Sham, S., and Hinton, J.F. (2001). Structures of gramicidins A, B, and C incorporated into sodium dodecyl sulfate micelles. Biochemistry *40*, 11676–11686.

Urry, D.W., Goodall, M.C., Glickson, J.D., and Mayers, D.F. (1971). The gramicidin A transmembrane channel: characteristics of head-to-head dimerized (L,D) helices. Proc. Natl. Acad. Sci. USA *68*, 1907–1911.

Woolf, T.B., Zuckerman, D.M., Lu, N., and Jang, H. (2004). Tools for channels: moving towards molecular calculations of gating and permeation in ion channel biophysics. J. Mol. Graph. Model. *22*, 359–368.

Woolley, G.A., and Wallace, B.A. (1992). Model ion channels: gramicidin and alamethicin. J. Membr. Biol. *129*, 109–136.

Wu, Y., Tian, X., Lu, M., Chen, M., Wang, Q., and Ma, J. (2005). Folding of small helical proteins assisted by small-angle X-Ray scattering profiles. Structure *13*, 1587–1597.